Chapter 2
Terahertz Sources and Detectors

This chapter describes techniques and systems regarding terahertz sources and detectors, mainly reviewing basic concepts and principles to help understand THz imaging instruments. The terahertz technologies outlined in this chapter provide background knowledge to the experimental work on the identification and reconstruction of terahertz spectroscopic data introduced later in this monograph. This chapter also covers the imaging modes, which involve both ultrafast pulsed systems and terahertz QCLs.

2.1 Introduction

Terahertz science has become increasingly popular in the recent decade due largely to the advent of time-domain spectroscopy (TDS) with ultrashort-pulse laser sources, which makes it possible for researchers to carry out time-resolved "far-infrared" (FIR) studies and to explore spectroscopy and imaging applications in the submillimeter wavelength regime.

Terahertz phenomena follow fundamental scientific interests. The goal of this chapter is to review the basic principles of different types of terahertz sources and detectors that are now possible with terahertz spectroscopy. They are fundamental to the understanding and conducting of the terahertz experiments, described later in the monograph.

This chapter will be organized as follows. Section 2.1 briefly introduces the history of terahertz radiation. Section 2.2 describes basic solid-state lasers, which are the principle components to achieve pulsed and continuous modes of terahertz spectroscopy. The topics range from conversion of ultrafast free-space laser pulses, to free-electron lasers (FELs), as well as QCLs. Section 2.3 introduces hardware devices for generating terahertz radiation. These terahertz emitters include EO emitters, PCA, planar antennas, and magnetic field enhancement devices, along

X. Yin et al., *Terahertz Imaging for Biomedical Applications: Pattern Recognition and Tomographic Reconstruction*, DOI 10.1007/978-1-4614-1821-4_2,

with terahertz photomixing. Section 2.4 discusses different types terahertz receivers based on different optical sampling methods. EO versus photoconductive and synchronous versus asynchronous sampling techniques are investigated.

2.2 The History of T-Rays

The term *terahertz* gained popularity among spectroscopists during the mid-1970s, (Kerecman 1973; Ashley and Palka 1973; Fleming 1974; Siegel 2002). A decade later, as a result of the efforts of many researchers and scientists, advanced techniques in optical rectification and photoconduction had been developed (Auston 1983; Smith et al. 1988) (see Sect. 2.4). These techniques made it possible to produce THz radiation directly using multimode lasers (van Exter et al. 1989; Cantor et al. 1981), such as Ti:sapphire-based lasers and FELs (Sect. 2.3.1). In 1989, Martin van Exter introduced a terahertz time-domain spectroscopy (THz-TDS) system (van Exter et al. 1989). This added momentum to the field of T-ray generation and detection, and some simple research began, including the extraction of material parameters from THz-TDS measurements.

Following this, Hu and Nuss in 1995 used a traditional scanned imaging system to acquire two-dimensional (2D) images. This was the beginning of geometric image formation of an object in the T-ray frequency range. TPI was viewed as a novel and promising method, especially applied to medical diagnostics (Löffler et al. 2001).

Subsequently, much effort was devoted to system improvement (Löffler et al. 2002). This included progress toward wavelet denoising of terahertz pulse imaging data (Ferguson and Abbott 2001b), denoising techniques for terahertz responses of biological samples (Duvillaret et al. 1996; Ferguson and Abbott 2001a), reducing measurement time (Zhao et al. 2002), and improving spatial (Chen et al. 2000) and depth resolution (Johnson et al. 2001). Improved systems made possible the development of new systematic approaches, such as time resolution of TPI in translation and reflection mode (Mittleman et al. 1997), dark-field TPI (Löffler et al. 2001), THz pulsed near-field image with good spatial resolution (Federici et al. 2002; Schade et al. 2004). In turn, T-ray CT technology was applied (Wu et al. 1996; Jiang and Zhang 1998a; Ferguson et al. 2002c,b). A review of further imaging modalities can be found in Chap. 3.

In the last 5 years, the rapid improvement of T-ray detectors and sources resulted in many technical advantages in THz-TDS and therefore opened up new fields of application. In particular, T-ray pulsed technology was used to image opaque objects. One promising application is the inspection of biomedical tissue. Examples are the separation of tumor cells from normal tissue (Woodward et al. 2002) ex vivo, and the study of in vivo normal to pathological samples of human skin (Gladkova et al. 2000), three-dimensional detection of tooth decay (Arnone et al. 2000), together with optical imaging and classification of a bird head (Löffler et al. 2002). Further aspects of spectroscopy and image analysis are reviewed in Chap. 4.

Time-domain TPI has the advantage of providing a broad frequency spectrum, but it incurs the high cost of an expensive femtosecond laser. CW imaging is attractive since it is a tunable, compact, and cost-effective system.

A coherent all-optoelectronic THz measurement system via photomixing techniques is normally implemented to produce tunable CW THz radiation. It was first demonstrated in 1998 by Verghese et al. (1998). Following this, Gu et al. (1999) pointed out that a tunable dual-wavelength external cavity laser diode was a promising laser source for the generation of tunable CW-THz radiation. Phase-sensitive CW THz imaging using diode lasers was introduced in 2004, with image capture rates comparable with those from state-of-the-art pulsed THz systems (Gregory et al. 2004). These diode lasers are cost effective for producing CW THz radiation. Additionally, Siebert et al. (2002) used two-color Ti:sapphire lasers to generate CW T-rays with an extension to biomedical applications. However, there exists an obvious drawback in that two expensive Ti:sapphire laser sources are required. The CW THz radiation mentioned above is generated by applying a pair of laser sources and photomixing techniques to achieve a tunable frequency range. For comparison, an entirely electronic generation and detection scheme is illustrated by Karpowicz et al. (2005b) and is a relatively compact CW THz imaging system with a few components. Such a system could easily be made portable, thus opening a much wider range of possible applications. However, as it lacks depth and phase information, the system only yields two-dimensional intensity images.

Photomixing techniques (in Sect. 2.4.3) applied to the generation of CW terahertz radiation, very severely limit the output power to $\sim 1\,\mu W$ at frequencies above 1 THz (Kim et al. 2006) mainly because of intrinsic parasitic impedance of the device and the impedance mismatch between the device and the radiating antenna (Darmo et al. 2004). QCLs operating in the terahertz range, however, have remained elusive for a long time until 2004, when the first terahertz QCLs were reported (Köhler et al. 2001). This is because of an insuperable barrier that exists in the phonon *reststrahlen* band, which causes difficulty in the further expansion to lower emission terahertz frequencies. Further, the development of a suitable waveguide is necessary (Sirtori et al. 1998a). It aims to confine light of the long wavelength within terahertz range to an epilayer compatible with molecular beam epitaxy technology and with low absorption losses onto the laser mode (Tredicucci et al. 2005). Recent novel design concepts have led to CW operation and high output powers (Rochat et al. 2002). In the recent years, terahertz QCLs have made rapid progress. They depend on chirped superlattices (Köhler et al. 2002a) and the surface plasmon concept (Köhler et al. 2002b) employed for a large optical confinement with low propagation losses, to recently, bound-to-continuum transitions and extraction of carriers via resonant phonon scattering (Williams et al. 2003). The lowest emission frequency is now ~ 1.39 THz. More recent progress of QCLs in terahertz range is presented in Sect. 2.3.3. One of considerable advantages of QCLs is the ability to tune the terahertz source to avoid regions of high water absorption. A relevant experiment has been conducted (Lee et al. 2006) with the atmospheric window selected at ~ 4.9 THz, to achieve real-time imaging of a dried seed pod at a 25-m

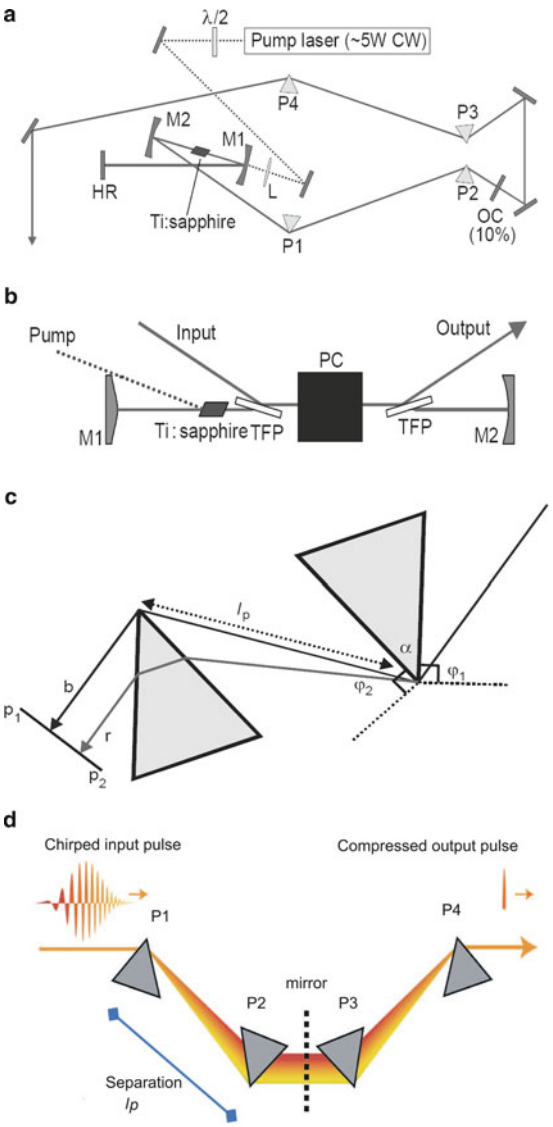

Fig. 2.1 Ti:sapphire-based lasers. (**a**) Diagram of a basic self-mode-locked Ti:sapphire oscillator shows the cavity layout. The output pulse is output from the end of the cavity dispersion, and then is tuned by a pair of matching extracavity prisms. (**b**) The schematics for regenerative amplification in Ti:sapphire oscillator. Ti:sapphire rod, 5 mm or less in length, is doped to absorb about 90% of the incident pump radiation. Two concave focusing mirrors, a pair of Kerr lenses, allow passive mode locking, where M1 is a high reflector and M2 is an output coupler. This pair of Kerr lenses forms the optical cavity. When light travels between the two lenses, the energy is accumulated in the interval of the gain medium, which causes a population inversion. The TFP indicates a thin-film polarizing beam splitter. The Pockel's cell (PC) is a Q switch and consists of voltage-controlled wave plates. The voltage rotates the plane of polarization by 90°, which results in the light being able to pass the medium. If the laser is Q-switched, a brief burst of light

standoff (see the relevant image mode in Sect. 3.2.3). Another important application of terahertz QCLs is in biomedical imaging; this is well illustrated by the work of Darmo et al. (2004) in imaging a rat brain section at 3.4 THz (Sect. 4.2.2).

Emission of relatively strong CW terahertz radiation from cuprate superconductors is carried out by Ozyuzer et al. (2007). Josephson junctions are stacked within the layered high-temperature superconductors. It is an important step toward filling this "terahertz gap" from 0.5 to 1.4 THz, in which the photomixing techniques and QC lasers can barely reach.

2.3 Laser Sources

2.3.1 Ti:Sapphire-Based Lasers

Ti:sapphire-based lasers were revolutionized in the 1990s, with the invention of self-mode-locking techniques. Currently, it is one of the most important laser sources for generating terahertz radiation (Reid and Fedosejevs 2005). Ti:sapphire-based lasers are frequently applied for the generation of pulsed terahertz radiation.

The principle of a Ti:sapphire-based laser is simply presented as follows. It consists of a rod of Ti:sapphire (titanium-sapphire), which can be pumped by a CW laser source. This light is focused into the Ti:sapphire rod collinearly with the laser axis through the back of a lightly silvered mirror. Dispersion arises from the variation of the refractive index of the crystal material across the gain bandwidth of the laser. The cavity dispersion output from the crystal material is Q-switched and self-mode-locked with the use of a pair of Kerr lenses (Brabec et al. 1992) as a saturable absorber and a Pockel's cell modulator. The schematic diagram regarding the Ti:sapphire pulsed laser oscillator is illustrated in Fig. 2.1b. The output from the laser oscillator, in Fig. 2.1a, is taken from the end that is opposite the dispersion-compensating prisms. This alignment of the prism pair creates a longer path for red wavelengths propagating through the prism material, as compared with the blue, which yields a negative dispersion effect. It is illustrated in Fig. 2.1c. If the prism separation, lp (defined tip to tip), is sufficiently large, the positive dispersion of the material can be balanced. The prism apex angle is cut to guarantee that at minimum deviation of the center wavelength, the incident angle is the Brewster

Fig. 2.1 (continued) excites population inversion and produces a stronger pulse. (**c**) Prism pairs are used in the control of dispersion; r and b indicate the relative paths of arbitrary long- and short-wavelength radiation. The incident (Brewster) angle at the prism face is labeled by φ_1. The light is reflected in the plane $p_1 - p_2$ in order to remove the spatial dispersion. (**a**)–(**c**): After Reid and Fedosejevs (2005). (**d**) Illustration of the optical path of the output cavity dispersion through the prism pairs. After Kafka and Baer (1987)

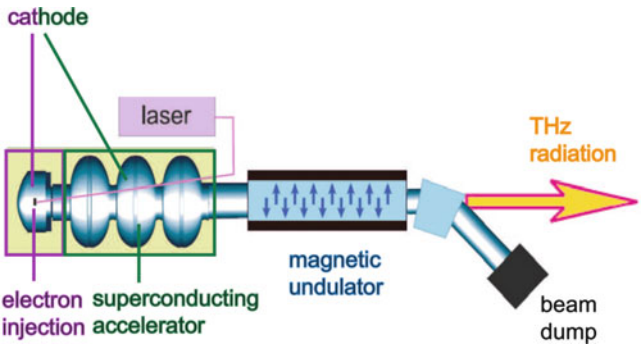

Fig. 2.2 A schematic of a THz free-electron laser. The schematic shows a short injector-accelerator combination compared to a stand FEL. After Grosse (2002)

angle. Figure 2.1d shows the optical path of the output cavity dispersion through the prism pairs. The compressed output pulse is finally achieved from chirped cavity dispersion by the application of prism pairs. The photograph of a Ti:sapphire-based laser is shown in Appendix D in Fig. D.1.

2.3.2 Free-Electron Lasers

Terahertz free-electron lasers (FELs) feature high intensity, combined with short pulse length, easy tunability, and variable pulse structure. These features are essential for biological and medical studies (Grosse 2002) and for the exploration of vibrational and configurational molecular transitions (Kato et al. 2000; Xie et al. 2002) in terahertz regime.

Unlike femtosecond lasers, that is, Ti:sapphire-based lasers, where quantum-mechanical principles are employed, the FEL (Krishnagopal et al. 2004) is a classical laser and converts part of the kinetic energy of the electrons into coherent electromagnetic radiation.

Figure 2.2 shows a schematic of a terahertz FEL. Two major components of the device are: electron accelerator and undulator. Generally, an undulator, such as in a linac or a synchrotron, is used to produce magnetic fields, which then drive an electron beam from an accelerator to achieve coherent terahertz pulsed radiation. Different from the setup of conventional FELs, the terahertz FELs accelerate electrons directly after they leave the photocathode (Volkov et al. 2000). The realization of a compact table-top full terahertz FEL system is now possible (Grosse 2002).

2.3.3 Terahertz Quantum Cascade Laser

Recent advances in nanotechnology have also led to the development of semiconductor-based THz sources: the terahertz QCL (Tonouchi 2007). Terahertz radiation is generated when electrons propagate the serial connection of coupled quantum wells. Quantum wells are formed in semiconductors by having a material, like gallium arsenide sandwiched between two layers of a material with a wider bandgap, such as $Al_xGa_{1-x}As$. These structures can be grown by molecular beam epitaxy with choice of the layer thickness, which determines the electron wave functions of the subbands. Unlike the conventional bandgap structure of semiconductor lasers, in QCLs, quantum confinement splits the conduction band into a number of distinct subbands (Köhler et al. 2002b; Faist et al. 1994). The energy spacing of the lasing subbands determines the radiation frequency, allowing in principle to produce light at arbitrarily long wavelengths.

Since the first QC laser was demonstrated at the much shorter wavelength of 4 μm (75 THz) at Bell Labs in 1994 (Faist et al. 1994), there have been over five types of terahertz QCLs since, due to the different mechanisms of electron energy relaxation processes (Vitiello et al. 2006). They are "chirped superlattice" (Williams 2007; Köhler et al. 2002b), "interlaced" (Köhler et al. 2004), and "resonant phonon" (Williams et al. 2004), "bound-to-continuum" (Vitiello et al. 2006) laser, as well as a recent design of two-color QCL with application of a magnetic field (Scalari et al. 2006).

The first THz QC laser with a photon energy less than the semiconductor optical phonon energy was demonstrated at 4.4 THz (equivalent to a wavelength of 67 μm) by Köhler et al. (2002b). A chirped superlattice (SL) technique was adopted to design the QCL active region, with advantage of very large current-carrying capabilities and optical powers (Tredicucci et al. 1998).

The bound-to-continuum (BTC) QCL has been proved to be successful in producing terahertz radiation with the replacement of the original chirped SL (CSL) design (Köhler et al. 2002b). The bound-to-continuum QCL takes place between an isolated upper state and a miniband with a small well adjacent to the injection barrier (Faist et al. 2001). The design combines the advantages of the three QW and superlattice active regions. It makes it possible to achieve selective injection into the upper state and fast extraction from the lower state. As a result, these designs display improved temperature and power performance compared with the CSL designs (Williams 2007; Alton 2005). A relevant experiment to use a BTC QCL for wavelet-based local reconstruction of a 3D polystyrene object is represented in Chap. 13. Figure 2.3a illustrates the design and performance of a bound-to-continuum QCL emitting at 2.9 THz. The laser was made at the University of Cambridge, by Jesse Alton, in collaboration with his colleagues (Alton 2005). The QC structure was grown by molecular beam epitaxy in a $GaAs/Al_{0.15}Ga_{0.85}As$ material system on a semi-insulating GaAs substrate. One period of the conduction band profile for each active region is displayed along with the calculated moduli squared of the most relevant wave functions.

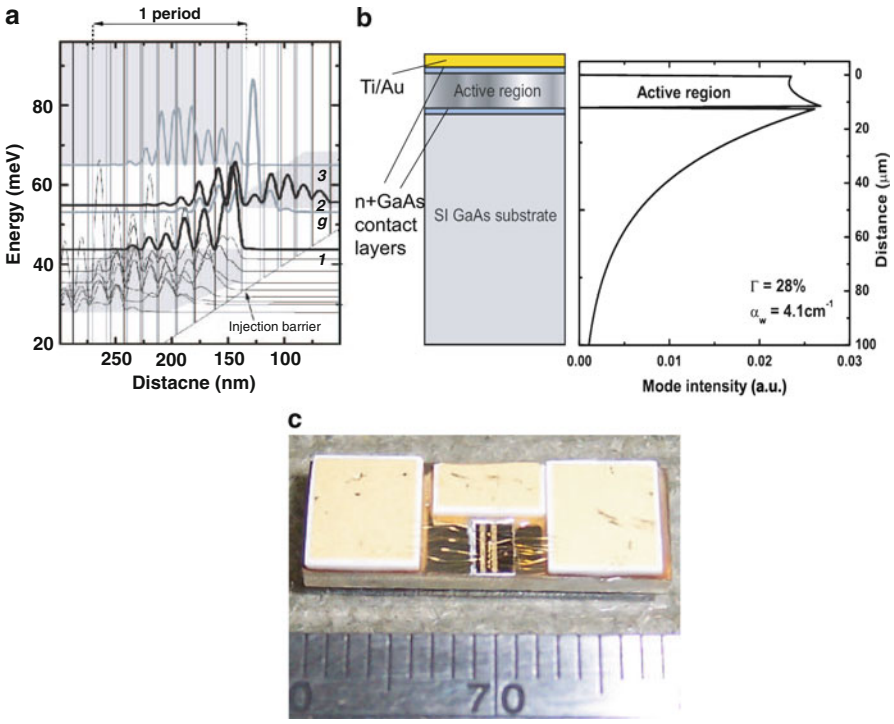

Fig. 2.3 The terahertz BTC quantum cascade laser scheme. (**a**) One period of the conduction band profile regarding a "vertical transition" design of the layer sequence. The upper, and lower state of the laser transition and the injector miniband ground state are labeled 2, 1, and g, respectively. The transition energy, given by the energy difference between 2 and 1, is 12 meV. At alignment, the wave functions of the upper and lower state are broadly overlapped. The upper state wave function is concentrated mainly in the two quantum wells adjacent to the injection barrier, reducing the overlap with the lower energy states in the injector miniband, thereby enhancing the non-radiative upper state lifetime. Electrons are injected into the upper state from state g through the injection barrier. The active region consists of 85 identical repeat periods. (**b**) Schematic representation of completed wafer cross section (*left*) and computed optical mode profile (*right*) along the growth axis. This waveguide is shown at $\lambda = 103\,\mu\text{m}$ (12 meV) and the yielded waveguide losses (α_w) of 4.1 cm^{-1} and a confinement factor (τ) of 28%. After Alton (2005). (**c**) Photograph of the BTC QCL (Figure courtesy of Lynn Gladden, Department of Chemical Engineering, The University of Cambridge, Cambridge, UK)

Figure 2.3b illustrates the waveguide design of the two BTC QCLs emitting at 2.9 THz. Both active regions are embedded between identical cladding layers: top contact layer is an 80-nm-thick GaAs, and bottom contact layer is a 700-nm-thick GaAs. The two contact layers are designed regarding the surface plasmon waveguide. The former has the same mode as a quasi-metallic layer (Köhler et al. 2002b) and the latter is completed by a Ti/Au metallization layer on top of the ridge cavity (the top contact layer). Figure 2.3c shows the photography of the finished BTC QCL.

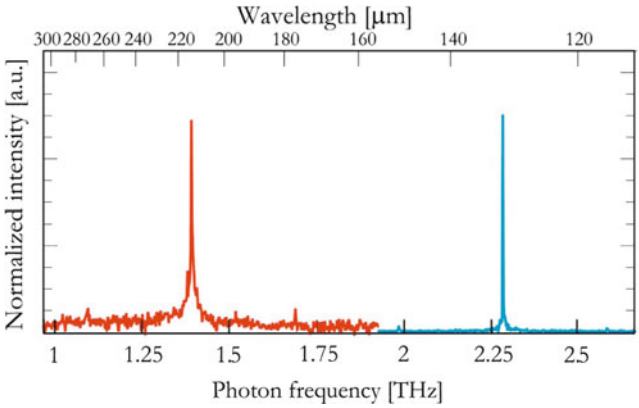

Fig. 2.4 Two-color terahertz quantum cascade laser spectrum. Illustration of the measured spectrum depending on the applied magnetic field. The line on the right indicates the emission frequency of 2.3–2.36 THz, and the line on the left corresponds to the emitted laser frequency at 1.39 THz. After Scalari et al. (2006)

In addition, a THz QCL utilizing alternating photon- and phonon-emitting stages has been developed to achieve efficient extraction of electrons from the lower laser level (Köhler et al. 2004). Though the impact of this interlaced photon–phonon cascade laser has been limited, they are particularly notable for achieving very long wavelength operation (Williams 2007). The other major active region type is the resonant-phonon (RP) scheme. The key design is to use resonant LO-phonon scattering to selectively depopulate the lower radiative level, while maintaining a long upper level lifetime. Owing to the lack of a miniband, the RP designs tend to have smaller oscillator strength (Williams et al. 2004).

At present, a QCL emitting at as low as 1.39 has been demonstrated by Scalari et al. (2006). An electrically switchable, two-color QCL emitting at 1.39 and 2.3 THz is realized by multiwavelength operation. A magnetic field is applied perpendicularly to the layers to increase the gain enabling laser action. The structure is based on a large single quantum well, and multi-wavelength operation is obtained by selectively injecting carriers via resonant tunneling into one of the excited states of this large quantum well (Sirtori et al. 1998b). Figure 2.4 shows the measured spectrum depending on the applied magnetic field.

2.4 Terahertz Semiconductor Sources (THz Emitters)

All-optical techniques have been recognized as an alternative approach to produce THz radiation (Davies et al. 2002) owing to the difficulties in fabricating solid-state THz sources. Semiconductor surfaces are widely used in conjunction with femtosecond visible/near-infrared lasers as THz emitters. Bulk EO rectification (difference frequency mixing) and ultrafast charge transport techniques have been

exploited. This section will review how semiconductor structures can be used to convert ultrashort (∼100 fs) near-infrared pulses into THz pulses, and then discuss one THz generation mechanism based on the ultrafast transport of electrons and holes at semiconductor surfaces.

2.4.1 Bulk Electrooptic Rectification (Optical Rectification)

Optical rectification is viewed as one of the main mechanisms to generate terahertz radiation using optical lasers (Tonouchi 2007). When a large peak electric field of a visible/near-infrared pulse is incident on an appropriate semiconductor crystal, it induces a second-order nonlinear susceptibility ($\chi^{(2)}$) of the crystal. The resulting nonlinear mixing of the Fourier components, produces a broadband extending up to THz frequencies.

Considering a time-dependent polarization induced in the THz frequency range, it is proportional to the intensity of the incident pump pulse (Davies et al. 2002) and the size of the second-order susceptibility. The generated THz frequency ω_{THz} is the difference between the pump pulse frequency ω_1 and the frequency of idling beam ω_2. This result holds when the energy conservation (sum frequency) $\omega_1 = \omega_2 + \omega_{\mathrm{THz}}$ and the phase matching condition $k_1 = k_2 \pm k_{\mathrm{THz}}$ between the induced THz field and the optical fields are satisfied (Schmuttenmaer 2004). The short duration of the incident pulse in the time domain allows a broad bandwidth (>10 THz) (Ma and Zhang 1993). Since the resulting pulses have a bandwidth of a few THz, the difference frequencies fall in the THz range (Schmuttenmaer 2004).

As the ultrafast pulse generates a polarization transient $p(t)$ in the EO crystal, according to the Hertzian dipole model, the resultant THz magnitude, $E_{\mathrm{THz}}(t)$, is given by the second time derivative of the polarization transient, $E_{\mathrm{THz}}(t) \propto \partial^2 p(t)/\partial^2 t$, where the time-domain polarization transient is expressed by $p(t) \propto \chi^{(2)} E^2_{\mathrm{opt}}(t)$, and $E_{\mathrm{opt}}(t)$ indicates the time series of optical pump pulse (Zhang et al. 1992). Figure 2.5a illustrates nonresonant optical rectification with an ultrafast laser pulse.

In a material with normal dispersion, the refractive index n increases with the frequency. Since $k = n\omega/c$, it turns out that the k_1-vector is too large, which causes difficulty in satisfying the phase matching condition. An alternative approach to obtain the phase matching condition is by exploiting the k-vectors of the extraordinary and the ordinary axes (Kubler et al. 2005). Further information on the nonlinear phase matching for terahertz generation can be found in the literature (Berger and Sirtori 2004; Sun et al. 2007).

To date, this mechanism has been used to generate THz radiation in a number of inorganic semiconducting materials including GaAs, GaSe, ZnTe (Ma and Zhang 1993; Saeta et al. 1993; Rice et al. 1994), CdTe, DAST, and $LiNbO_3$, although more effective materials are being explored (Davies et al. 2002). Zinc telluride (ZnnTe) is regarded as the most popular EO material due to its physical durability and excellent phase-matching properties (Rice et al. 1994). The organic crystal DAST has a very

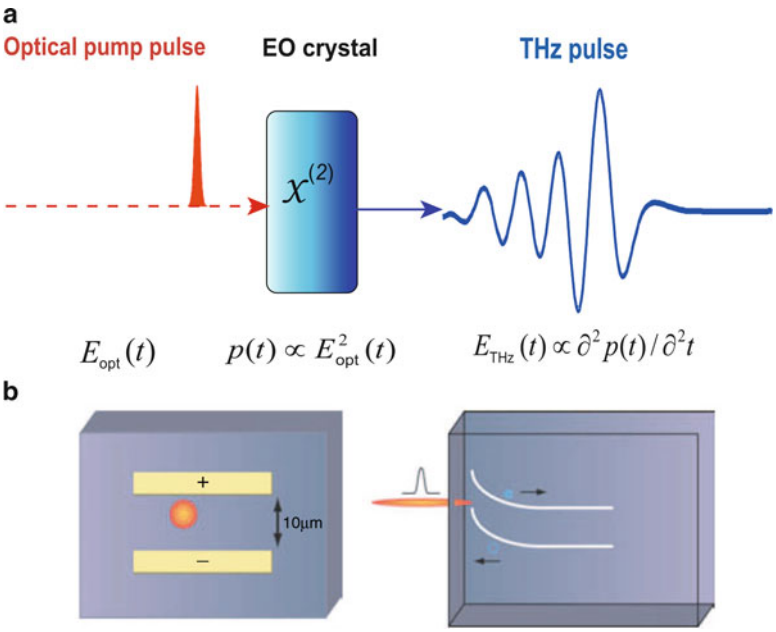

Fig. 2.5 Optical rectification and ultrafast charge transport schemes. (**a**) Optical rectification (OR) is a second-order nonlinear effect, whereby an ultrafast electric field pulse is rectified in a $\chi^{(2)}$ medium, in this case an electrooptic (EO) crystal. The ultrafast pump pulse induces a transient polarization, $p(t)$, which in turn emits a T-ray bandwidth pulse. The time evolution of the T-ray pulse is given by the second time derivative of the polarization transient, $E_{\mathrm{THz}}(t) \propto \partial^2 p(t)/\partial^2 t$. (**b**) Illustration of schematic diagrams regarding two THz emitters via applying the ultrafast charge transport scheme. Photoexcited carriers are generated by a focused visible/near-infrared laser pulse and then are accelerated and radiate in an electric field. On the left hand side, the field is provided by a lateral antenna structure; on the right-hand side, the intrinsic semiconductor surface depletion/accumulation field is exploited. After Davies et al. (2002)

large EO coefficient (Zhang et al. 1992), but is difficult to use experimentally owing to its hygroscopic character. Saturation of OR due to second harmonic generation of the pump beam at high optical fluences has been studied in ZnTe (Sun et al. 2000), $LiTaO_3$, $LiNbO_3$, and DAST (Carrig et al. 1995).

2.4.2 Ultrafast Charge Transport

In an absorbing medium, such as an $\langle 110 \rangle$ or $\langle 111 \rangle$ oriented semiconductor, terahertz radiation can be produced by means of "nonresonant" optical rectification (Dakovski and Shan 2005). But if the photon energy of the ultrafast pulse is higher than the semiconductor bandgap, photons are absorbed, and electron–hole pairs are created close to the surface of the generation crystal. The terahertz radiation is

generated primarily as the result of another mechanism—ultrafast charge transport. In this process, an appropriate electric field is introduced to accelerate photoexcited electron–hole pairs within a semiconductor structure, leading to generation of a THz pulse.

Typically, suitable surface fields are realized in two ways. On the left-hand side of Fig. 2.5b, a lateral antenna comprising two electrodes deposited onto a semiconductor surface is shown. A large electric field is applied between the electrodes. The incident laser pulse is focused between the two electrodes, and then creates electro–hole pairs. The free carriers are accelerated by the static field along the field direction and form a transient photocurrent (Zhang and Auston 1992). The emission bandwidth can be modified by appropriate band structure engineering (Leitenstorfer et al. 1999; Davies et al. 2002).

A second mechanism is illustrated on the right-hand side of Fig. 2.5b. This was first demonstrated by Zhang et al. (1990). A surface electric field is built up when an ultrafast laser pulse with the photon energy is greater than the semiconductor bandgap. The surface depletion field is vertical to the semiconductor surface, which drives the ultrafast charge transport. Compared to wide bandgap semiconductors, narrow bandgap semiconductors show an enhanced photo-Dember effect, owing to these characteristics with respect to high electron mobilities and large amount of kinetic energy of the photoexcited electrons. The efficient mechanism of the ultrafast buildup and relaxation of the photo-Dember field results in the generation of THz radiation in narrow bandgap semiconductors (Gu et al. 2002). The emitted power and bandwidth for this generation of terahertz radiation is determined by the temperature and properties of the semiconductor crystal, as well as the energy, pulse width, and flux of the incident laser pulse (Davies et al. 2002).

Recently, there has been enormous interest in the mechanism of magnetic field enhancement of terahertz (THz) emission from photoexcited carriers in the surface depletion region of a semiconductor (Izumida et al. 1999; Weiss et al. 2000; McLaughlin et al. 2000). In this case, the optical rectification process is negligible owing to the crystal orientations and the large amount of excess photon energies in the excitation. The analysis of the THz emission process is based on the Drude–Lorentz model (Shan et al. 2001; Weiss et al. 2000). In the absence of a magnetic field, the emitted THz radiation is completely polarized by transverse-magnetic (TM), caused by the surface depletion field. As the magnetic field is increased, a transverse electric (TE) component is introduced, and the emitted THz radiation becomes elliptically polarized. Both TE and TM power are significantly enhanced in the additional magnetic field. The emission can be measured either by an incoherent bolometric detection scheme or by coherent EO sampling (Davies et al. 2002). Figure 2.6 illustrates the schematic of the experimental geometry based on the magnitude enhancement scheme.

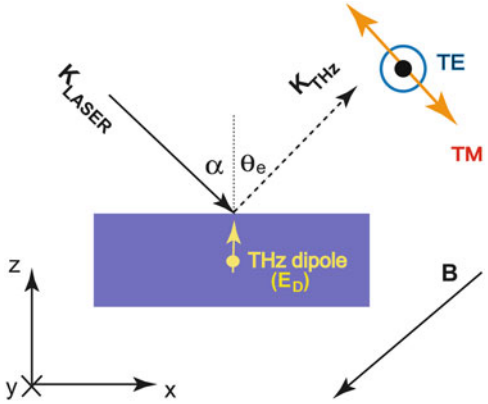

Fig. 2.6 Magnetic-field-enhanced generation of T-rays in semiconductor surfaces. A femtosecond laser pulse is incident on the semiconductor surface at angle α, resulting in a depletion field (E_D) vertical to the surface of the semiconductor. The carrier acceleration by the depletion field generates two components: the electric field E_x and E_z of the THz pulse. Both components determine the measured THz signal, which is polarized in the x–z plane. The emitted THz radiation is measured at angle θ_e. The direction of the applied magnetic field is shown by the vector **B**. The emitted THz radiation is collected parallel to the applied magnetic field and perpendicular to the incident beam. The TM mode and the vertical TE mode are labeled by a *yellow double arrow line* and a *blue circle* with a *black dot* inside. After Davies et al. (2002)

2.4.3 Terahertz Photomixing

Without requesting bulky and expensive femtosecond lasers, photomixing offers an alternative method for generating terahertz radiation. Photomixing can be achieved using two CW lasers, and interference produced between two CW lasers (Brown et al. 1993, 1995) contains different above-bandgap (visible or near-infrared) wavelengths. In these all-photoconductive systems, inexpensive, compact, and tunable diode lasers (Gregory et al. 2004; Vitiello et al. 2006) can be used as the laser sources.

The photomixing techniques-based CW-THz emitters and detectors mainly consist of a photoconductor and an antenna. The photoconductor can be viewed as a combination of a photoconductive switch (semiconductor) and a photomixer. The electrodes and photoconductive gap are generically termed the photomixer. The electrodes are designed as the structure of interdigitated fingers coupled to a photoconductive gap. A schematic of a typical CW-THz device is shown in Fig. 2.6a.

As for a fully optoelectronic detection of the terahertz CW radiation, a component separated from the original laser beam can be used to gate the receiver. A rapid-scan delay line allows collection of the detected terahertz waveforms. A standard 60° "bow-tie" antenna, shown in the insets of Fig. 2.6b, and hyper-hemispherical silicon lenses can couple the radiation in and out of the semiconductors (Gregory et al. 2004).

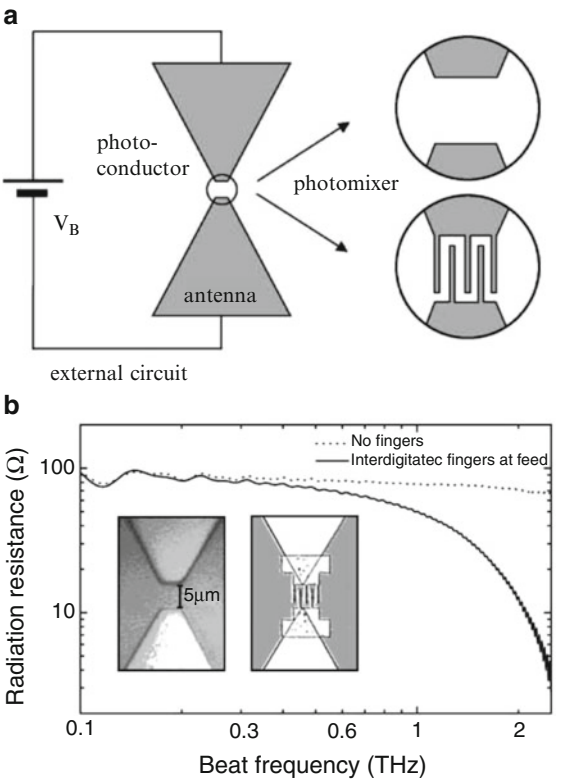

Fig. 2.7 Photomixing schematics. (**a**) A schematic of a typical CW-THz device. (**b**) Two *insets* are the micrographs of the actual structures: a 60° "bow-tie" antenna structure with a bare photoconductive gap and the electrode structure linked to the antenna with the design of interdigitated fingers. For both structures, the antenna radiation impedance is plotted as a function of frequency. After Gregory et al. (2004)

2.5 Terahertz Optical Sampling Techniques

Optical sampling (also called optoelectronic sampling) refers to a class of techniques, which are used to perform time-resolved measurements of terahertz responses (Schmidt-Langhorst and Weber 2005). The optical signals, usually in the form of ultrashort pulses, are used to probe the terahertz electrical field, and ultimately, extract sample information from terahertz responses. In terahertz detection systems, there are four main sampling techniques: free-space EO sampling, antenna detection, synchronous, and asynchronous optical sampling.

2.5.1 Coherent Terahertz Radiation Detection

Coherent terahertz radiation detection techniques involve free-space EOS and antenna detection. EOS shows good sensitivity and a broad bandwidth, compared to antenna detection. Electro-optic sampling is an optoelectronic technique of optical

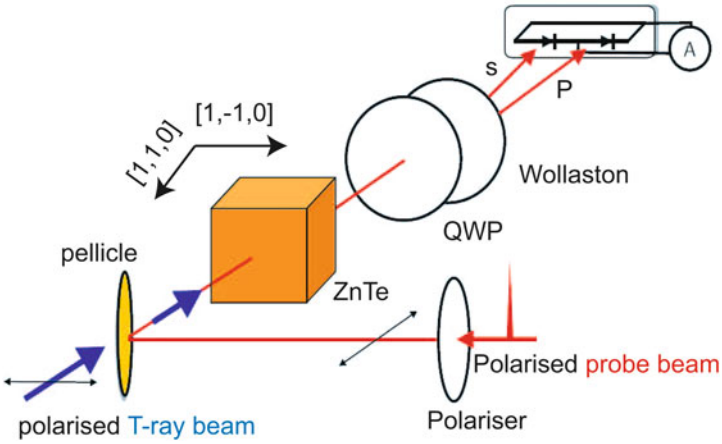

Fig. 2.8 Sketch of an electrooptic sampling setup. The polarized T-ray electric field induces a birefringence in the detector, according to the $\chi^{(2)}$ coefficient of the specific crystallographic orientation of the crystal (Chen and Zhang 2001). Produced birefringence in turn rotates the polarization of the probe beam, after the probe beam transmits through the EO detector collinearly with the pump beam (incident T-ray response), directed by a pellicle beam splitter. A Wollaston beam splitter, directs the two polarizations to balanced photodiodes. A quarter-wave plate (QWP) is rotated to balance the difference current to zero for zero T-ray field in the EO crystal. After Mickan (2003)

sampling, realized via exploiting the linear EO effect (also called the Pockel effect). The electric field is exercised by an ultrashort optical pulse, an EO probe beam, and the influence between the electric field and the terahertz radiation occurs during only a short time interval. This effect is usually a change of polarization, which is turned into a change of optical power by a polarizer. A polarizing beam splitter, which can be viewed as a second polarizer rotated 90° from the first polarizer, is used to split and direct the polarization rotation that the THz field induces on the probe beam and to achieve intensity modulation of the polarization. This is a typical crossed-polarizer detection method (Saleh and Teich 1991; Yariv 1991). A pair of balanced silicon photodiodes is used to analyze the split polarization rotations. The slow variation in the arrival time of the probe pulse, that is, sequential sampling of a repetitive signal, results in the measurement of a full waveform of a periodic signal. It is observed that EO detection is noise sensitive, and there exists a clear trade-off between the noise sensitivity and frequency response. It is determined by the choice of crystal and its thickness (Cai et al. 1998). Figure 2.8 illustrates the sketch of an EO sampling setup.

Photoconductive sampling is an optical sampling technique, which is achieved by using photoconductive switches. It is found that the antenna detection scheme always has a better SNR than EOS, with the chopping frequency at a few kilohertz (Cai et al. 1998). Photoconductive detection is similar to photoconductive generation. A short probe laser pulse can close an electrical connection for a very short time. A bias electric field across the antenna leads is generated by the

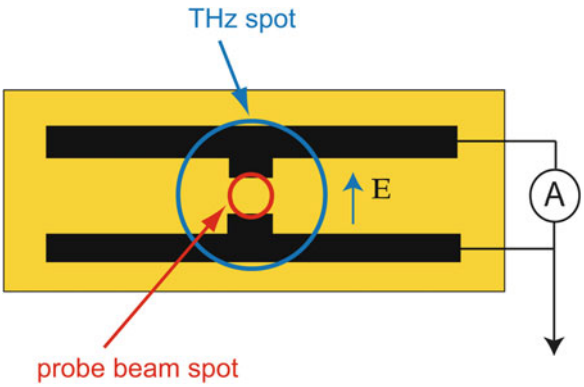

Fig. 2.9 Sketch of a PCA used for photoconductive sampling. This sketch shows a photoconductive dipole antenna used for T-ray detection. The large T-ray spot (shown as a *blue circle*) biases the electrodes with a free-space electric field. The probe spot is focused into the biased region of the antenna substrate. The fs-duration probe switches the electrodes with transient photocarriers, allowing a current to flow, which is detected by an ammeter. The current flow is proportional to the applied T-ray field. After Mickan (2003)

electric field of the THz pulse focused onto the antenna. The PCA directly detects a photocurrent induced by the incident THz field. Figure 2.9 is the sketch of a PCA used for photoconductive sampling. The presence of the THz electric field generates current across the antenna leads, which is usually amplified using a low-bandwidth amplifier. This amplified current is the measured parameter which corresponds to the THz field strength. Again, the carriers in the semiconductor substrate have an extremely short lifetime. Thus, the THz electric field strength is only sampled for an extremely short time interval (fs) of the entire electric field waveform, the temporal position of which can be adjusted via an optical delay line (see Fig. 2.10).

2.5.2 Synchronous and Asynchronous Optical Sampling

Synchronous optical sampling is an important implement in a terahertz pump-probe system. In this system, data are recorded in the time domain via different delay times. The varied delay time is achieved by several approaches: (1) traditional scanner with a motorized scanning stage, (2) raster scanning, and (3) mechanical scanning devices. This approach, called synchronous sampling, needs to guarantee a correct match between each acquired waveform and the location of the measured object.

Asynchronous optical sampling (ASOPS) is a technique for fast measurements of time-domain spectroscopy (Yasui et al. 2005; Bartels et al. 2007). The application of this technique has been successfully demonstrated in the field of THz-TDS, that is, for DNA analysis (Janke et al. 2005; Kistner et al. 2007) and water vapor

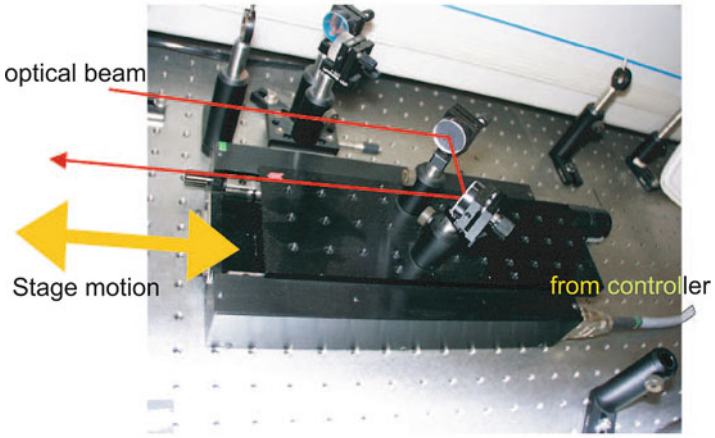

Fig. 2.10 Pump-probe delay stage. The delay stage pictured here is the essential element in pump-probe experiments, of which T-ray spectroscopy is one example. The stage is used to sweep the ultrafast probe pulses over the temporal profile of the free-space T-ray pulse, thereby sampling the entire T-ray waveform. The stage motion is coordinated with the detection electronics via a computer and general purpose interface bus (GPIB). After Mickan (2003)

detection (Brown et al. 2006). This technique adopts two different mode-locked lasers with a slight difference in pulse repetition rates. The two different pulses automatically provide a temporally varying delay. The scan rate is determined by the different pulse repetition rates. Only the low enough scan rate is effective to allow for a sufficient temporal resolution, which is then limited by the detection bandwidth (not by the pulse duration). A high pulse repetition rate helps, as long as a sufficiently large temporal range scanning is available. The large number of the recorded spectra makes it possible either to record data for many samples per second (e.g., to obtain position-dependent transmission spectra or even two-dimensional transmission images) or to average many spectra data from a single sample within a few seconds, aiming to reduce detection noise to a very low level. Fast-detection electronic devices allow for recording thousands of transmission spectra, ranging from virtually zero to several terahertz, within 1 s. Asynchronous sampling avoids mechanical noise of the delay time and position-dependent mode size, but at the cost of requiring two lasers instead of one (Chan et al. 2007).

2.6 Chapter Summary

This chapter has broadly described the common techniques and systems for terahertz detection and generation. Several advanced T-ray sources which are primarily used for current popular terahertz research include (1) pulsed T-rays based on ultra-fast laser sources; (2) high-frequency electronic sources, for their integration

into existing electronic technology, to achieve low-power CW operation; and (3) QCLs, for their small size and tunability, to realize CW operation. The pulsed nature of ultrafast T-ray systems provides high SNRs, broad bandwidth, and low average power, making them ideal tools to study biological and medical materials. However, QCLs as terahertz narrowband laser sources show deeper penetration, due to higher average power, which complements TPI systems. Based on instruments reviewed in this chapter, the following chapter reviews T-ray imaging modalities, which underpins THz tomography. Such systems then open up the possibility for imaging and pattern recognition of heterogeneous layers within a target object (Chap. 4).

http://www.springer.com/978-1-4614-1820-7

Terahertz Imaging for Biomedical Applications
Pattern Recognition and Tomographic Reconstruction
Yin, X.; Ng, B.; Abbott, D.
2012, XVI, 316 p., Hardcover
ISBN: 978-1-4614-1820-7